NANO LETTERS

2008
Vol. 8, No. 6
1689-1694

Study of Single Silicon Quantum Dots' Band Gap and Single-Electron Charging Energies by Room Temperature Scanning Tunneling Microscopy

Bashir Zaknoon and Gad Bahir*

Department of Electrical Engineering, Technion-Israel Institute of Technology, Haifa 32000, Israel

Cecile Saguy

Solid State Institute, Technion-Israel Institute of Technology, Haifa 32000, Israel

Rachel Edrei and Alon Hoffman*

Schulich Faculty of Chemistry, Technion-Israel Institute of Technology, Haifa 32000, Israel

Rajesh A. Rao, Ramachandran Muralidhar, and Ko-Min Chang

Freescale Semiconductor Incorporated, 3501 Ed. Bluestein Boulevard, Austin, Texas 78750

Received March 2, 2008; Revised Manuscript Received April 23, 2008

ABSTRACT

Scanning tunneling spectroscopy in the shell-filling regime was carried out at room temperature to investigate the size dependence of the band gap and single-electron charging energy of single Si quantum dots (QDs). The results are compared with model calculation. A 12-fold multiple staircase structure was observed for a QD of about 4.3 nm diameter, reflecting the degeneracy of the first energy level, as expected from theoretical calculations. The systematic broadening of the tunneling spectroscopy peaks with decreasing dot diameter is attributed to the reduced barrier height for smaller dot sizes and to the splitting of the first energy level.

Single-electron transistors (SETs) are expected to become basic structural elements in future ultrahigh density and ultralow-power very large-scale integration (VLSI) design. These devices are based on the controllable transfer of single electrons through small conducting "islands" or dots.[1–3] By taking advantage of the Coulomb blockade effect in controlling the transfer of individual electrons, the SETs could lead to single-electron logic and single-electron memory-based devices. Recently, self-assembled silicon quantum dots (QDs), which were grown by chemical vapor deposition (CVD) techniques[4,5] for producing nonvolatile memories, have been studied.[6,7] The focus was, in particular, on the influence of the QD density, size,[6] and tunneling barriers[8] on the memory device performance. In parallel, recent interest in elucidating the electronic structure of these nanocrystals has rapidly increased. Indeed, the programming and reliability properties of future QD-based producing nonvolatile memory devices will be strongly influenced by the position of the first energy level and the charging energy of electrons.[5]

Scanning tunneling spectroscopy (STS) provides a direct method to study the individual energy levels of single nanocrystals and quantum dots. In particular, STS is important for a single Si dot study where complementary optical techniques such as photoluminescence are difficult and are strongly affected by the dots surrounding. In addition, it is difficult to separately investigate electron and hole energy levels by optical spectroscopy. STS has been used to probe the energy levels and charging energies (Coulomb blockade) of semiconductor QDs (InAs,[9,10] CdSe,[11,12] and PbSe[13]). The majority of these studies were focused on the electronic structures of II−VI and III−V compound semiconductors

* Corresponding author. E-mail: bahir@ee.technion.ac.il (G.B.) and choffman@tx.technion.ac.il (A.H.).

10.1021/nl080625b CCC: $40.75
Published on Web 05/17/2008

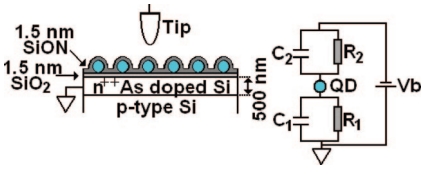

Figure 1. Schematic description of the sample structure (left) and the double barrier tunnel junction equivalent circuit (right).

colloidal QDs. Recently, Coulomb blockade for an ensemble of Si QDs was observed at room temperature by macroscopic electrical measurements.[14] Evidence for the existence of a Coulomb blockade and staircase structure in single Si QDs was reported at low temperature and room temperature using STS.[15] To date, a STS systematic experimental study of the electronic level scheme and the energy-level degeneracy of strain induced self-assembled single QDs, in general, and CVD-grown single Si QDs, in particular, has not yet been reported.

In this work, the special design of the sample (described in the next paragraph) enabled us to investigate the electronic structure and Coulomb repulsion of well-defined surface-terminated single Si QDs, 2−6 nm in diameter, by STS at room temperature. The fine structure above the band gap was interpreted in terms of single-electron charging energy in the tip−QD−substrate double barrier tunnel junction (DBTJ) and of quantized energy levels of the Si QD and their degeneracy. The relations between the measured band gap energy, the single-electron charging energy, and the size of the crystalline Si QDs were in good agreement with quantum confinement models.[16–18] Interpretation of the STS results is based on the model for single-electron tunneling and the conventional effective capacitive model.[19,20]

The samples studied in this work have been designed and fabricated according to scanning tunneling microscopy (STM) technique requirements. A 1.5 nm thin thermal SiO_2 layer was grown on an arsenic heavily doped n-type Si wafer ($\sim 10^{20}$ cm^{-3}). After oxidation, Si QDs were grown by atomistic nucleation using low pressure CVD and then passivated at 850 °C in an NO ambient, forming a thin N-rich oxide shell on the surface of the QDs. The detailed process and modeling of the Si QDs' growth is described elsewhere.[5] Scanning electron microscopy (SEM) and atomic force microscopy (AFM) images revealed that the density of the QDs is 8×10^{11} cm^{-2} and their mean size is 4 nm. Cross section transmission electron microscopy (TEM) images of our sample demonstrated that the QDs have a crystalline core, with a semispherical shape. The STM/STS measurements were performed in a variable temperature STM Omicron system in a vacuum of 4×10^{-11} torr. Prior to any STS measurement, the sample was in situ annealed overnight at 500 °C.

For studying STS, a DBTJ was obtained by positioning the tip over a single QD, as schematically shown in Figure 1, and was modeled by using the parameters C_1, C_2, R_1, and R_2.[9,20,21] The QD−substrate junction parameters (C_1 and R_1) cannot be modified, whereas the tip−QD junction parameters (C_2 and R_2) can be easily modified by changing the applied voltage (V_b) or the tunneling current set point, hence changing the tip dot distance. To experimentally observe, at room temperature, effects due to the discrete nature of a charge in an isolated QD, the single-electron charging energy, E_C, of a QD and the electronic level separation must exceed the thermal energy fluctuation, k_BT. The value of E_C is e^2/C_T, where $C_T = C_1 + C_{dot} + C_2$. C_{dot} is the self-capacitance of the QD; its value is estimated below. In addition, the width of the tunneling current peaks, which depends on the tunneling rate, should be smaller than E_C. An important parameter in tunneling spectroscopy is the number of additional electrons (holes) in the Si QD. In the limiting case, termed "shell filling spectroscopy", where the rate of tunneling into the QD, $\Gamma_2 \alpha 1/R_2$ is comparable to the electron escape rate from the Si QD, $\Gamma_1 \alpha 1/R_1$, the degeneracy of the levels is lifted because of the interactions between the carriers accumulating in the QD.[12,20] This condition is achieved here by the existence of an oxide layer between the QDs and the substrate, whose thickness is roughly equal to the thickness of the upper passivation oxynitride shell. In the neutral state, when the QD is not charged, the voltage division between the two junctions is given by $V_2/V_1 = C_1/C_2$ and $V_b = V_1 + V_2$. To obtain quantitative information from the tunneling spectra, the voltage division between the two junctions should be such that most of the applied bias voltage (~90%) will fall on the tip−QD junction ($C_1/C_2 \sim 10$; e.g., $C_2 = 0.13$ aF, $C_1 = 1.3$ aF for 4 nm Si QD, as will be shown later). Under these conditions, the conduction band (valence band) appears at positive (negative) bias, and the real QD level separations can be extracted directly from the peak spacing in the dI/dV versus V characteristics.

Figure 2a shows a STM topography image of a 100×100 nm^2 area of the sample. Topography images were obtained with sample bias of −7 V and with a tunneling current set point of 0.1 nA. The observed QDs' height ranges from 2 to 8 nm. The density shape and size of the Si nanocrystals on the same sample are shown in the SEM image presented in Figure 2b. Most QDs are isolated with lateral dimension, including the SiON cap, ranges from 2 to 10 nm. Because of the inherent property of the STM tip, the measured lateral size of QDs, as observed by STM is larger than the expected real dimension, deduced from HRTEM cross section (not shown here), SEM measurements Figure 2b and the following references.[5,6,8] Taking this into consideration, for the rest of the work, we determined the QD diameter from the STM-measured height, assuming a nearly spherical dot shape. Special care was taken to select a current−voltage set point that provides a highly asymmetric DBTJ ($C_1 \gg C_2$) while maintaining a "shell filling" condition, as can be seen from the constant separation between charging peaks in the dI/dV spectra. The STS experiments were performed with sample bias set point of −1.5 V and with a tunneling current set point of 0.2 nA. Typically, few $I-V$ curves were acquired above a single dot and their reproducibility was checked. We found that the dI/dV versus V curves were reproducible, but small fluctuations in the peak positions were observed. The measured random small shifts are attributed to "spectral diffusion" induced by electrostatic

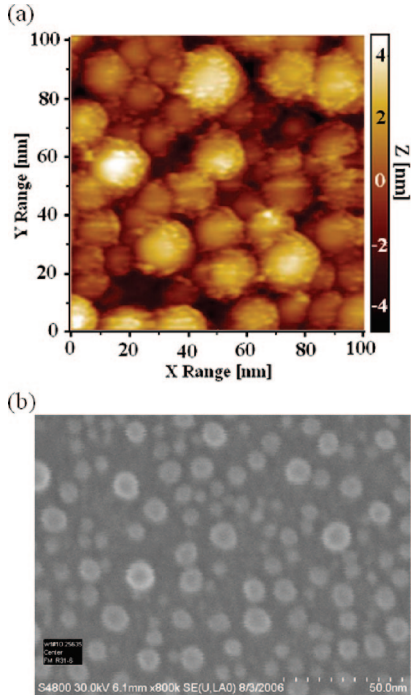

Figure 2. (a) 100 × 100 nm^2 STM topography image of QD sample taken at sample bias of −7 V and set-point current of 0.1 nA. (b) 150 × 100 nm^2 SEM image of the same sample exhibits isolated quantum dots with diameter ranges from 2 to 10 nm.

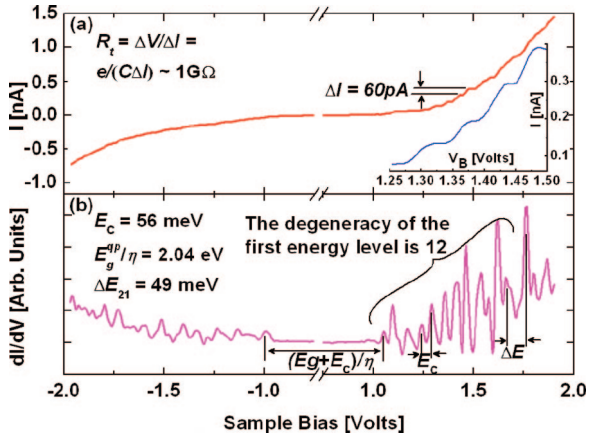

Figure 3. (a) STS measurement on single Si QD, 4.3 ± 0.25 nm in diameter, acquired at room temperature, showing the tunneling $I-V$ characteristic. The inset shows the extended part of the tunneling $I-V$ curve. (b) Corresponding dI/dV − V tunneling spectrum. The arrows depict the main energy separations: E_g, the single-particle QD band gap, E_C, the charging energy, and $\Delta E = \Delta E_{21} + E_C$, the sum of the level spacing and charging energies.

reconfiguration in the QD surrounding medium. All data presented below were acquired at room temperature. Figure 3a shows an $I-V$ curve on a 4.3 ± 0.25 nm diameter Si QD. This curve, typical of others, shows a region of suppressed tunneling current around zero bias, followed by a series of steps at both negative and positive bias. From a value of ΔI = 60 pA for the current staircase steps, as extracted from Figure 3a, and C_T = 2.23 aF, as estimated below, the total tunneling resistance of the two junctions, R_t, can be estimated as ~1−5 GΩ ($R_t = e/(C_T\Delta I)$). This

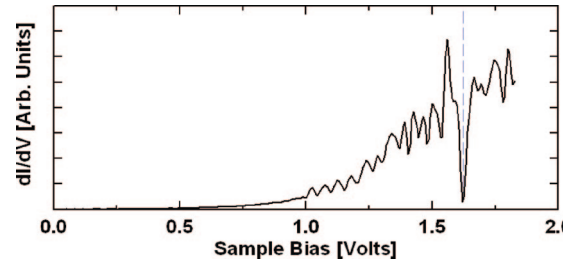

Figure 4. Positive bias side of the dI/dV vs V tunneling spectra at room temperature for 4.5 ± 0.25 nm diameter Si quantum dot. The observed multiplet is consistent with the degeneracy of the first bulk conduction band energy level, which has 12-fold degenerate states owing to spin and the Si six-valley degeneracy. The vertical dashed line marks the space between the first energy level and the second one. The separation between the two groups of peaks, represents the sum of the level spacing ΔE_{21} and the charging energy E_C.

value is larger than the quantum resistance, h/e^2 ~ 25.81 kΩ, meaning that quantum fluctuations are not expected to mask single-electron charging effects at room temperature. Figure 3b displays the corresponding differential conductance spectrum, dI/dV versus V, obtained by the numerical derivation of the digitally filtered $I-V$ curve. Using the low noise set up of the Omicron system, we could measure the tunneling $I-V$ current directly without lock-in amplification. The Si QD energy band gap, E_g (or the single-particle gap[22]), was extracted from the observed spacing between the highest valence band and the lowest conduction band peaks, which is equal to the normalized quasi-particle band gap[22] E_g^{qp}/η, where $E_g^{qp} = E_g + E_c$, $\eta = C_1/(C_1 + C_2)$, and E_C is the direct Coulomb energy, neglecting other smaller contributions.[22] The data displayed in Figure 3b clearly show that the conduction band (positive bias side) exhibits 12 closely resonant tunneling peaks separated by an average spacing of E_C = 56 meV, followed by a larger spacing, ΔE = 105 meV, and three additional nearly equidistant peaks. We attribute this group of 12 peaks to tunneling through the lowest conduction band state, where the spacing corresponds to single-electron charging energy, E_C = 56 meV. This result was reproducibly obtained on "large" ~4.5 nm diameter QDs. As an example, Figure 4, measured on a 4.5 ± 0.25 nm diameter Si QD, shows very similar features of 12 peaks in the dI/dV differential conductance spectrum with slightly smaller charging energy of 49 meV. The observed multiplet is consistent with the degeneracy of the first bulk conduction band energy level, which has 12-fold degenerate states owing to spin and the Si six-valley degeneracy.[17,18,22] Theoretical calculations[22] have shown that, for a QD of that size, the 12-fold degenerate first energy level in the bulk splits into three sublevels, separated by less than 5 meV, owing to the break of translational symmetry in small QDs. Our measurement resolution is limited by the thermal energy fluctuation that did not allow us to experimentally observe this splitting. To turn back to Figure 3b, the higher multiplet with 3 peaks may be ascribed to the conduction band second energy level. The separation between the two groups of peaks, ΔE = 105 meV, represents the sum of the level spacing ΔE_{21} and the charging energy E_C. A value for $\Delta E_{21} = \Delta E - E_C$ = 49

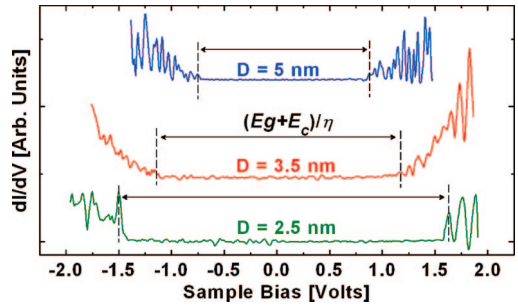

Figure 5. d*I*/d*V* vs *V* tunneling spectrum of three representative Si QDs with different sizes. For clarity of presentation, we offset the spectra along the vertical direction. The applied bias was kept smaller than the quasiparticle gap for each dot to avoid injection of both electron and holes at large positive bias.[20]

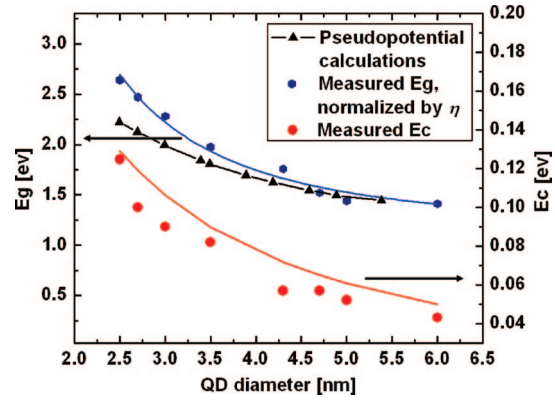

Figure 6. Measured single-particle gap, E_g, vs QD diameter (blue dots) and the EMA fit for E_g (solid blue line). The black triangles show the single-particle gap empirical pseudopotential calculations data, taken from ref 17. The measured Coulomb charging energy, E_C, versus QD diameter (red dots) and capacitive model calculations for E_C (solid red line).

meV is thus obtained. This value of ΔE_{21} is in discrepancy with the value obtained by the theoretical calculations (about 100 meV) for unoxidized and H-terminated Si QDs.[18] We attribute this difference to the fact that the electronic properties of the QDs are strongly affected by the surrounding passivation shell.[22,23] On the negative bias side, tunneling through filled QD levels in the valence band takes place. The multiplicity in this case reflects a complicated QD valence band level spectrum, and in contrast with the conduction band, it cannot be clearly assigned to a specific degeneracy. The 12-peak degeneracy was observed only on the relatively large dots, ~4.5 nm, where the expected splitting of the lower energy level is small (<5 meV). The reason that we did not observe 12 peaks in small dots could be due to the larger splitting of the first energy level. For a dot size of 5 nm or larger, the separation between charging peaks in the d*I*/d*V* versus *V* spectra was comparable with the experimental uncertainty.

Figure 5 shows a set of d*I*/d*V* versus *V* tunneling conductance spectrum corresponding to room temperature STS measurements on Si QDs with diameters of 2.5, 3.5, and 5 ± 0.25 nm. The applied bias was kept smaller than the quasiparticle gap for each dot to avoid injection of both electron and holes at large positive bias.[20] A few important features can be clearly observed from this figure: (a) The d*I*/d*V* versus *V* tunneling spectra, are symmetric around the zero bias voltage region. This is because the QDs are intrinsic, and the work function of the tungsten tip (4.55 eV) is approximately equal to the work function of intrinsic Si (4.52 eV). Thus, for zero bias voltage, the Fermi energy level of the tungsten tip lies in the middle of the QD energy band gap.

(b) As expected, large-size Si QDs have smaller band gaps and smaller single-electron charging energies compared with smaller ones. Single-particle band gaps of 2.64, 1.97, and 1.44 eV and average single-electron charging energies in the CB of 125, 82, and 53 meV were directly extracted from the d*I*/d*V* versus *V* spectrum, for the 2.5, 3.5, and 5 ± 0.25 nm QDs, respectively. Note that the spacing between the tunneling peaks attributed to the single-electron charging slightly vary for the same QD; this behavior may result from mesoscopic fluctuations in the charging energy.[24] In order to minimize these fluctuations, we took the average of the measured spacing values as the value of E_C. The fluctuations in peak spacing within charging multiplets were studied on metal[24] and semiconductor[25] QDs and found to be Gaussian, with a width that scales with E_C.

(c) For smaller QDs, the tunneling peak widths in the conduction band are broader. The peak widths are well-above our experimental resolution. This effect can be explained by the first energy level splitting and by the dependence of Γ_1, the escape tunneling rate from the QD to the Si substrate, on the QD size, as argued in ref 25 where wider tunneling peaks were reported for smaller-size colloidal InAs QDs. In our case, Γ_1 can be extracted from simple-square tunneling barrier geometry approximation. By assuming that z, the thickness of the SiO_2 layer for junction 1, is the same for all QDs (z = 1.5 nm), the dependence of Γ_1 on the QD size comes therefore from the variation of the tunneling effective barrier height, $U - E$. The values U and E, both evaluated relatively to the bottom of the conduction band for the Si substrate, are the barrier height ($U \approx 3.2$ eV for the SiO_2/Si conduction band offset) and the first electronic level confined in the Si QD, respectively. This effective barrier height is reduced for smaller Si QDs because of the increase in E due to quantum confinement, whereas U remains constant.

Figure 6 (blue dots, left *y* axis) exhibits the measured single-particle energy band gap (E_g) vs the QD diameter, as deduced from STS measurements. The Si QD single-particle band gap, E_g, was extracted from the observed spacing between the highest valence band and the lowest conduction band peaks, which is equal the normalized quasi-particle band gap E_g^{qp}/η, where $E_g^{qp} = E_g + E_c$, and $\eta = C_1/(C_1 + C_2)$. Since C_1 and C_2 depend on QD size, η is not constant during the measurements of different QDs. Therefore, the capacitance values were calculated separately for each quantum dot as described below. According to our capacitance evaluation, we found that η ranges between 0.88 (for D = 2.5 nm) and 0.92 (for D = 6 nm). An increase in the measured energy band gap is observed when the QD diameter is reduced. On the basis of the single-band effective

mass approximation (EMA) theory, the band gap energy of the three-dimensionally confined Si QDs can be expressed as $E_g = E_{bulk} + Q/D$,[2,17] where E_{bulk} is the band gap energy of the bulk crystalline Si, Q is the quantum confinement parameter, and D is the diameter of the Si QD in nanometers. As shown in Figure 6, the least-squares fit (solid blue line) of the data shows a fit with the equation, $E_g = 1.136 + 9.75/D^2$ for the band gap energy of crystalline Si QDs. The fitted bulk band gap energy of 1.136 eV approaches 1.12 eV, the bulk crystalline Si band gap. From the photoluminescence of the Si QD ensemble, a fit to the band gap energy with equation $E_g = 1.13 + 13.9/D^2$ has been reported recently.[26] The differences between the two works are possibly related to the fact that the electronic properties of the QDs are strongly affected by the dot shape and surrounding passivation shell.[23]

The interaction energy of the electron in semiconductor QDs with its own polarization charges, $\sum(D)$, at the surface of the dielectric sphere of diameter D, and the additional upward energy shift $U(D)$, corresponding to the average Coulomb interaction between electrons in the dielectric sphere, are strongly dependent on the ratio between the dielectric constants of Si dot, ε_{Si}, and the surrounding dielectric sphere ε_{out}.[20,22] It is shown in ref 20 that, when $\varepsilon_{Si} \gg \varepsilon_{out}$, $U(D) = 2\sum(D)$ and the metallic capacitive model can be applied to semiconductor nanocrystals where $U \sim e^2/C_T = E_C$. In our study, $\varepsilon_{Si} \sim 11.8$ and $\varepsilon_{out} < 3.9$ (the SiO_2 dielectric constant), taking into account that the dot-surrounding sphere is composed from thin layers of SiO_2, SiON, and vacuum due to the tip−dot distance. Our simple model is justified on this basis. A comparison between the measured dot single-particle band gap and pseudopotential calculations[17] is shown in Figure 6 (black triangles). A good agreement was shown for large dots; however, for smaller dots, the experimental results are consistently higher (about 10%). We can attribute this effect to possible experimental errors in determining the exact QD diameter, errors in η evaluation for small dots, and to differences between the model's assumptions regarding the dielectric constants mismatch and the real ones.

Figure 6 (red dots, right y axis) shows the measured single-electron charging energy for the first conduction band energy level versus the QD diameter and the calculated single-electron charging energy $E_C = e^2/C_T$ (solid red line). An increase in E_C is observed with a reduction in the QD diameter. As expected, a smaller QD has a smaller capacitance; thus, larger energy is needed to charge the QD with an additional single electron. Our results are in good agreement with ref 15, reporting STS at room temperature and low temperature on single Si QDs deposited on 1.2 nm thermal oxide. To fit the experimental values of E_C displayed in Figure 6 to model, one should estimate the different capacitances. The estimation of C_T is based on a simple electrostatic model that considers the tip−QD−substrate geometry, as shown in Figure 1.

A capacitor model describing the capacitance between a metal sphere and a grounded plane[26] is applied to estimate the value of C_1, as given by eq 1.

$$C_1 = 2\pi\varepsilon_{SiO_2} D \cdot \left[1 + \frac{D}{4l} + \frac{(D/4l)^2}{1-(D/4l)^2}\right] \quad (1)$$

where D is the dot diameter and l is the distance between the center of the QD and the metal plan. The value C_2 is evaluated by an approximate solution of the capacitance between two metal spheres,[27] where the tip termination is approximated to be a small sphere whose diameter is evaluated from STM topography measurements on the QDs. The SPIP™ software[28] was used for these measurements. The self-capacitance of the QD, C_{dot}, is roughly given by $2\pi\varepsilon_{SiO_2}D$.

The systematic error between the experimental single-electron charging energy, E_C, and the calculated data, shown in Figure 6, originates from our simple electrostatic model that assumes that the QD and the substrate are metals, in addition to possible systematic experimental errors.

In conclusion, we carried out a detailed study of the electronic properties of single Si QDs grown by low pressure CVD on 1.5 nm SiO_2 grown on a highly doped Si substrate. The electronic level structure and the single-electron charging effect of a single Si QD was investigated at room temperature by shell filling tunneling spectroscopy. We found that the degeneracy of the first energy level of "large" ~4.5 nm diameter QDs is 12, consistent with theoretical predictions. Good agreement was also found between the experimental data regarding the dependence of the Si QD band gap and the single-electron charging energy on the QDs' diameter and the model calculations.

Acknowledgment. We thank Dr. A. Zunger for fruitful discussions. This work was supported in part by a grant from the Israeli Ministry of Science.

References

(1) Devoret, M. H; Esteve, D.; Urbina, C. *Nature* **1992**, *360*, 547.
(2) Tiwari, S; Rana, F.; Hanafi, H.; Hartsein, A.; Rabbe, E. F.; Chan, K. *Appl. Phys. Lett.* **1996**, *68*, 1377.
(3) L, J.; Leobandung, E.; Chou, S. Y. *Science* **1997**, *275*, 649.
(4) Baron, T.; Martin, F.; Mur, P.; Wyon, C.; Dupuy, M. *J. Cryst. Growth* **2000**, *209*, 1004.
(5) Steimle, R. F.; Muralidhar, R.; Rao, R. A.; Saad, M.; Swift, C. T; Yater, J.; Hradsky, B.; Straub, S.; Gasquet, H.; Vishnubholta, L.; Prinz, E. J.; Merchant, T.; Acred, B.; Chang, K.; White, B. E., Jr. *J. Microelectronics Reliability* **2007**, *47*, 585.
(6) Rao, R. A.; Gasquet, H. P.; Steimle, R. F.; Rinkenberger, G.; Straub, S.; Muralidhar, R.; Anderson, S. G. H.; Yater, J. A; Ledezma, J. C.; Hamilton, J.; Acred, B.; Swift, C. T.; Hradsky, B.; Peschke, J.; Saad, M.; E. J., Prinz; Chang, K. M.; White, B. E., Jr. *Solid-State Electronics* **2005**, *49*, 1722.
(7) Lombardo, S; De Salvo, B.; Gerardi, C.; Baron, T *Microelectron. Eng.* **2004**, *72*, 88.
(8) Baik, S. J.; Choi, S.; Chung, U.-In.; Moon, J. T. *Solid-State Electron.* **2004**, *48*, 1475.
(9) Banin, U.; Cao, Y. W.; Katz, D.; Millo, O. *Nature* **1999**, *400*, 542.
(10) Maltezopouslos, T; Bolz, A.; Meyer, C.; Heyn, C.; Hansen, W.; Morgenstern, M.; Wiesendanger, R. *Phys. Rev. Lett.* **2003**, *91*, 196804.
(11) Katz, D.; Wizansky, T.; Millo, O.; Rothenberg, E.; Mokari, T.; Banin, U. *Phys. Rev. Lett.* **2002**, *89*, 086801.
(12) Jdira, L.; Liljeroth, P.; Stoffels, E.; Vanmaekelbergh, D.; Speller, S. *Phys. Rev. B.* **2006**, *73*, 115305.
(13) Liljeroth, P.; Zeijlmans van Emmichoven, P. A.; Hickey, S. G.; Weller, H.; Allan, G.; Vanmaekelbergh, D. *Phys. Rev. Lett.* **2005**, *95*, 086801.
(14) Cho, C. H.; Kim, B. H.; Park, S. J. *Appl. Phys. Lett.* **2006**, *89*, 13116.
(15) Baron, T.; Gentile, P.; Magnea, N.; Mur, P. *Appl. Phys. Lett.* **2001**, *79*, 1175.
(16) Niquet, Y. M.; Delerue, C.; Allan, G.; Lanoo, M. *Phys. Rev. B* **2000**, *62*, 5109.

(17) Reboredo, F. A.; Zunger, A. *Phys. Rev. B* **2000**, *62*, 2614.
(18) See, J.; Dollfus, P.; Galdin, S. *Phys. Rev. B* **2002**, *66*, 193307.
(19) Averin, D. V.; Korotkov, A. N.; Likharev, K. K. *Phys. Rev. B* **1991**, *44*, 6199.
(20) Niquet, Y. M.; Delerue, C.; Allan, G. *Phys. Rev B.* **2002**, *65*, 165334.
(21) Millo, O.; Banin, U. *Annu. Rev. Phys. Chem.* **2003**, *54*, 465.
(22) Franceschetti, A.; Zunger, A. *Phys. Rev. B* **2000**, *62*, 2614.
(23) Nishida, M. *Semicond. Sci. Technol.* **2006**, *21*, 443.
(24) Sivan, U.; Berkovits, R.; Aloni, Y.; Prus, O.; Auerbach, A.; Ben-Yoseph, G. *Phys. Rev. Lett.* **1996**, *77*, 1123.
(25) Millo, O.; Katz, D.; Cao, Y. W.; Banin, U. *Phys. Rev. B* **2000**, *61*, 16773.
(26) Kim, T. W.; Cho, C. H.; Kim, B. H.; Park, S. J. *Appl. Phys. Lett.* **2006**, *88*, 123102.
(27) Sarid, D. *Exploring Scanning Probe Microscopy with Mathematica*; Wiley−Interscience: new York, 2006; revised and expanded edition.
(28) *Scanning Probe Image processing*, SPIP™; Image Metrology A/Shttp://www.imagemet.com/index.php.

NL080625B